Nanoscale

Accepted Manuscript

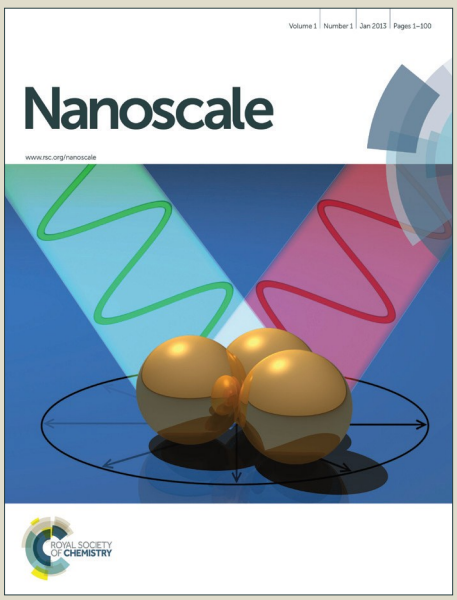

ROYAL SOCIETY OF CHEMISTRY

www.rsc.org/nanoscale

Journal Name

COMMUNICATION

The shape evolution from Pt_xCo_y@Co cubes to Pt_xCo_y multicubes for selective hydrogenation of α,β-unsaturated aldehyde

Received 00th January 20xx,
Accepted 00th January 20xx

DOI: 10.1039/x0xx00000x

www.rsc.org/

Shuangshuang Huang,[a,b] Nating Yang,[a,b] Minfeng Huo,[a,c] Yuhan Sun*[a,c] and Yan Zhu*[a,c]

We report the synthesis of Pt_xCo_y@Co cubes and Pt_xCo_y multicubes through the previous structure as seed precursors to induce the formation of the latter. Here Pt_xCo_y nanocrystals underwent a shape evolution from core-shell structure to multicubes under an identical synthetic condition via the previous structure serving as a seed precursor to induce the formation of the latter. Pt_xCo_y@Co cubes can be viewed as Pt_xCo_y octapods core coated by Co atoms shell, and exhibited complete selectivity towards C=C bond of unsaturated aldehyde. Co shell of Pt_xCo_y@Co was further substituted by introducing Pt atoms, followed by the successive deposition of Pt on Pt_xCo_y and the interdiffusion between Pt and Co, leading to the formation of multicubes. Such multicubes gave rise to the superior catalytic activity with higher selectivity for C=O bond of unsaturated aldehyde, compared to pure Pt nanocubes and a commercial Pt/C catalyst.

Predictable control of the heterogeneous nucleation of two alien metals anisotropic products is really challenging, owing to the difficulty in accessing structurally well-defined precursors. Pt-Ni nanocrystals with fantastic structures such as polyhedrons,[1-5] nanocages,[6,7] core-shell,[8,9] and concave/convex particles,[10,11] have been reported, and their excellent behavior on the olefins hydrogenation and oxygen reduction reaction has drawn the researchers' interesting on.[4,12] However, few significant advance in the heterogeneous nucleation of Pt-Co nanocrystals is mentioned in the related literatures, thus the scarcity of structural diversification of Pt-Co nanocrystals has precluded the widely development in catalytic research of Pt-Co bimetal. Some investigations carried out on Pt-Co bimetallic catalysts are focused on the α,β-unsaturated aldehydes,[13,14] and the resulting unsaturated alcohols from C=O hydrogenation and saturated aldehydes from C=C hydrogenation are valuable intermediates for the production of perfumes, flavors and food spices.[15,16] The selectivity to unsaturated alcohols is improved when Co atoms are associated with Pt atoms in a particle,[17,18] in that the electropositive Co is supposed to act as an electron-donor to increase the electron density on the surface Pt atoms, thus decreasing the probability of C=C bond activation and simultaneously promoting the activation of C=O bond.[19] However, we did not gain a deep understanding about the structural effect of Pt-Co bimetallic nanocrystals on the final products of α,β-unsaturated aldehydes. In consideration of the difficulty in the concomitant nucleation of Pt and Co under a synthetic system, we need to make the best of the different nucleation rate of Pt and Co to direct the shape variation and formation of well-defined Pt-Co nanocrystals.

Drawing inspiration from the seed-mediated approach of molecular chemistry,[20,21] herein our attention is firstly given to the structural control of seed precursors of Pt-Co nanocrystals. In an early stage of synthetic procedure, Pt_xCo_y dendrite-like multipods were formed in the reaction solution, and then went through a site-selected deposition of Co atoms on the interstices between adjacent pods of the multipods, followed by a coating of Co adatoms on the surface of these multipods. Finally Pt_xCo_y@Co cubes were obtained, generating a core-shell structure, that is, an octapod core made of Pt-Co alloy and a shell made of Co. Meanwhile Pt_xCo_y@Co cubes also can act as seed precursors to confine the structural variation of Pt-Co nanocrystals and induce the formation of Pt_xCo_y multicubes via the substitution Pt for Co and the interdiffusion between Pt and Co. Especially, the ability to control the selective hydrogenation process of α,β-saturated aldehyde is acquired by tuning the shape variation of Pt-Co nanocrystals. Pt_xCo_y@Co achieved almost complete selectivity for C=C bond of unsaturated aldehyde, whereas Pt_xCo_y multicubes gave rise to the more product from C=O bond hydrogenation. Furthermore, Pt_xCo_y multicubes showed higher activity of hydrogenation, compared to Pt nanocubes and a commercial Pt/C catalyst.

Fig. 1a shows a transmission electron microscopy (TEM) image of the as-synthesized Pt_1Co_2@Co cubes. An ultrathin shell with about 2 nm and a cubic core with about 25 nm can be clearly discernible in the inset of Fig. 1a because of their difference in

[a] CAS key laboratory of Low-Carbon Conversion Science and Engineering, Shanghai Advanced Research Institute, Chinese Academy of Sciences, Shanghai 201210, China. E-mail: zhuy@sari.ac.cn; sunyh@sari.ac.cn
[b] University of Chinese Academy of Sciences, Beijing 100049, China.
[c] School of Physical Science and Technology, ShanghaiTech University, Shanghai 201210, China.

Electronic Supplementary Information (ESI) available: [details of any supplementary information available should be included here]. See DOI: 10.1039/x0xx00000x

electron density. High-resolution TEM studies from which the labeled area in Fig.1a is taken indicate that the lattice spacing of 0.20 nm on the shell can be assigned to the {111} lattice fringe of faced-centered cubic Co (Fig. 1b). For the core, the lattice fringe direction with d-spacing of 0.18 nm obtained on HRTEM corresponds to the {200} planes of Pt-Co alloy, which was smaller than the {200} planes of Pt crystal. It could be attributed to the decrease of lattice distance along the increase of the amount of smaller Co atoms (1.26 Å) in place of Pt atoms (1.36 Å).[22] The rings resulting from selected-area electron diffraction further support the alloy nature of Pt-Co in the core (Fig. S1). Energy-dispersive X-ray spectroscopy (EDS) mapping analysis (Fig. 1c) points to the distribution range of Pt and Co in the core-shell cubes, revealing Co-rich on the shell of the particle and the interstices between adjacent pods. Fig. 1d presents the line-scanning profile of an individual cube with a 25 nm octapod core and a 2 nm shell, which clearly shows the space distribution of Co and Pt in the cube. Along the scan direction, a nearly symmetric line profile featuring a pronounced volcano of the Pt profile at the core region can be observed from the peak line. A hillock feature of the Co profile along the scan direction points towards a smooth continuous compositional transition between core and shell, indicating that Co exists in the core and shell. It is worth to note that Co atoms are preferentially centered in the shell as well as the interstice of the octapod. It implies that during the formation of the core-shell structure, Co atoms should selectively deposit in the interstices between adjacent pods and outermost layer of octapods.

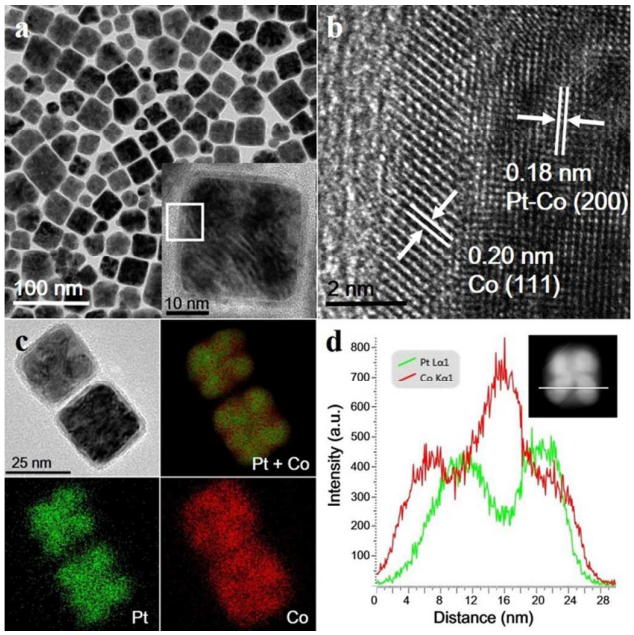

Fig. 1 (a) TEM image of Pt_1Co_2@Co cubes and inset is TEM image of a single cube. (b) High-resolution TEM image taken from a circled area of a cube. (c) EDS elemental mapping of Pt (green) and Co (red) for two cubes. (d) Line-scanning profiles across an individual cube.

The time-sequential evolution experiment gave us insight into the morphological variation of Pt-Co nanocrystals (Fig. 2 and S2). At the initial deposition, the multipods of mainly Pt-Co nanocrystals are obtained from the fact that the lattice spacing of 0.19 nm is assigned to the {200} lattice fringe of Pt-Co, were formed in the reaction solution (Fig. 2a and its inset). At 10 min after CO introduction, the multipods were still made of Pt-Co alloy (Fig. 2b and its inset; see Supporting Information and corresponding Fig. S2-3 about the role of CO). From 10 to 15 min, the shape transferred from multipods to ill-defined octapods (Fig. 2c). From 15 to 20 min, ill-defined octapods transferred to well-defined octapods (Fig. 2c-d). At 20 min, the interstices between adjacent pods started to be filled with Co, which was obtained by the color contrast from the different electron density of Pt and Co (Fig. 2d and its inset). The core-shell structure was observed at 25 min, and the shell was enclosed by Co and the core was bounded by Pt-Co (Fig. 2e and its inset). After 25 min, the core-shell structure has no obvious change, as shown in Fig. 2f and S4. During the reaction process, the atom ratio of Pt to Co decreased with time (insets of Fig. 2), demonstrating that the nucleation rate of Pt is faster than that of Co in the reaction. The investigation clearly proved that the formation of multipods of Pt-Co nanocrystals preceded that of core-shell cubes, and the former went through a site-selected deposition of Co atoms on the interstices of the octapods and on the surface of these octapods, causing the formation of Pt_xCo_y@Co cubes.

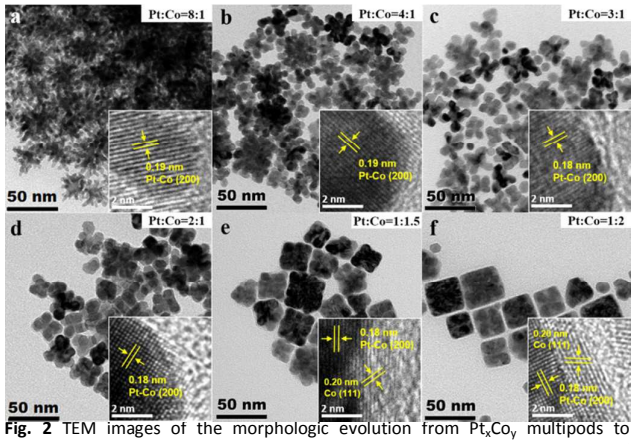

Fig. 2 TEM images of the morphologic evolution from Pt_xCo_y multipods to Pt_xCo_y@Co cubes with reaction time. Insets are the corresponding atom ratios of Pt to Co from EDS analysis and HRTEM images. The reaction time was (a) before CO introduction, (b) 10 min, (c) 15 min, (d) 20 min, (e) 25 min, and (f) 30 min.

The exposing of all almost non-nobel metal atoms on the surface is not of benefit to the utilization efficientcy of Pt metal on the increase of the catalytic activity for hydrogenation reactions. Therefore, we further prepared a multicubic structure of Pt-Co nanocrystals with high proportion of Pt atoms exposed on the surface via Pt_xCo_y@Co cubes as seed precusors to direct the formation of Pt_xCo_y multicubes. Based on a "substitution" mechanism,[23] Pt adatoms can substitute for some Co atoms on the surface, leading to the disappearance of Co-rich shell. So, we put some Pt_xCo_y@Co cubes into a mixed solution of oleylamine and oleic acid, followed by excessive $Pt(acetylacetone)_2$ addition. The morphology evolution and chemical composition during the synthesitic process were examined. As shown in Fig. 3b, when the reaction time was less than 1 min, the change of shapes was not obvious. When the time was 2 min, the outlayers of cubes became flimsy and the octapods were in focus, because of the

substitution of Pt for Co (Fig. 3c). As the time was extended to 5 min, the Co-rich shell disappeared (Fig. 3d). Owing to the existence of excessive Pt^{2+} ions in the solution, Pt atoms were to continue depositing on the faces of these pods. Meanwhile, the Pt and Co in the pods suffered the intermixing. Finally, the curved surface of octapods became flat through the deposition of Pt, leading to the formation of the multicube, where each multicube is constructed with eight cubes (Fig. 3e). However, when the reaction time was longer like 30 min, the more Pt was deposited on the surface of multicubes, resulting in the evolution of multicubes to larger cubes (Fig. 3f). The atomic ratios of Pt to Co increased with the reaction time (insets of Fig. 3), manifesting that the amount of Pt deposition on these particles increased with the reaction time (insets of Fig. 3). The HRTEM studies also demostrated the substitution and interdiffusion of Pt and Co (insets of Fig. 3). Before 1 min, Co (111) planes can be clearly observed on the shell (insets of Fig. 3a-b), while 0.20 nm lattice spacing of Co (111) planes was not found on the outlayers of these particles after 2 min reaction. Notably, the clear Pt-Co (200) lattice fringe direction with d-spacing of 0.18 nm reveals the formation of Pt-Co alloy, corfirming the intermixing and alloying between Pt and Co.

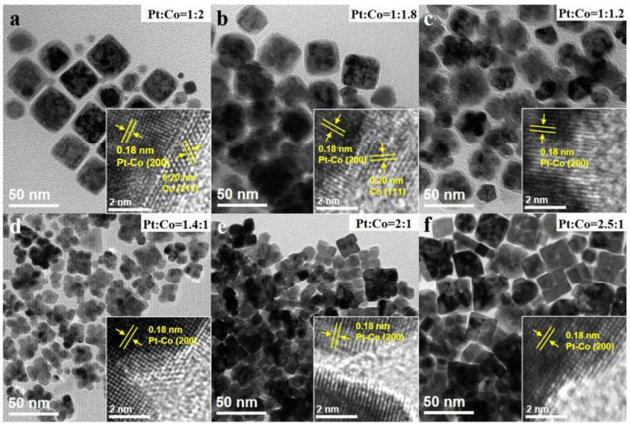

Fig. 3 TEM images of the morphologic evolution from Pt_xCo_y@Co cubes to Pt_xCo_y multicubes with reaction time. Insets are the corresponding atom ratios of Pt to Co and HRTEM images. The reaction time was (a) 0 min, (b) ~30 s, (c) 2 min, (d) 5 min, (e) 15 min, (f) 30 min.

A representative TEM image of Pt_2Co_1 multicubes is shown in Fig. 4a. A clear multicubic structure is demostrated by HRTEM (Fig. 4b), and a multicube is well constructed with eight cubes. Each cube has an approximate 10 nm edge length and the dominant exposed facets of such cubes are {100}, which are the only planes normal to the set of (200) planes with lattice space of 0.18 nm (Fig. 4c). Noted that some high-index facets, such as {130}, exist in the junction area between the adjacent cubic components of a multicube (Fig. 4c). From the element maps of Pt and Co in multicubes (Fig. 4d), we can observe that Pt is rich on the outside of multicubes and homogeneorous space distribution of Pt and Co in the inside of multicubes. It identifies that some Co atoms on the shell of particles and the interstices between adjacent pods are substituted by Pt adatoms, followed by remaining Co atoms on the shell and interstices are interdiffusing with entering Pt atoms.

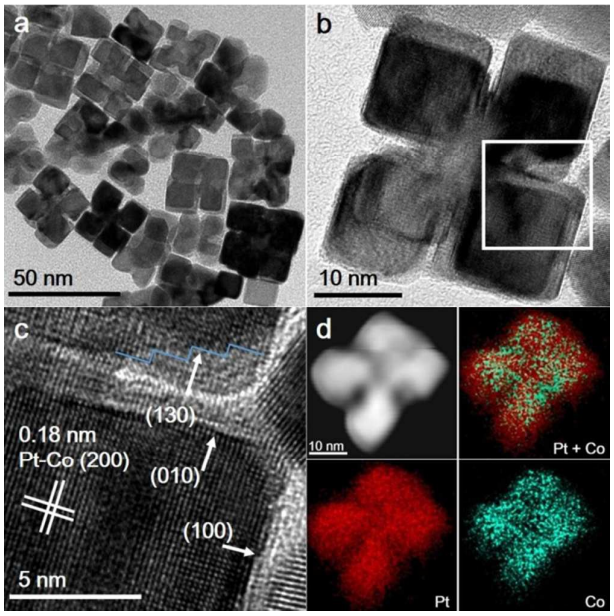

Fig. 4 (a) TEM image of Pt_2Co_1 multicubes. (b) TEM image of a multicube. (c) HRTEM image taken from a circled area of (b). (d) EDS elemental mapping of Pt (red) and Co (blue) in a typical Pt_2Co_1 multicube.

We chose the selective hydrogenation of α,β-unsaturated aldehyde like cinnamaldehyde as a targe to evaluate the catalytic performance of Pt_1Co_2@Co cubes and Pt_2Co_1 multicubes. Pure Pt nanocubes and a commerial Pt/C catalyst were also tested to provide a contrast for catalytic activity and selectivity of cinnamaldehyde hydrogenation. TEM image of Pt nanocubes was shown in Fig. S5. Pt_2Co_1 multicubes exhibited a higher catalytic activity for cinnamaldehyde hydrogenation, compared to Pt nanocubes and Pt/C catalyst, whereas Pt_1Co_2@Co cubes gave rise to the lowest activity among the four catalysts, owning to the enshrouding of active species by Co-rich shell. Interestingly, almost alone C=C bond of cinnamaldehyde was hydrogenated on the Pt_1Co_2@Co cubes (Fig. 5b), together with trace saturated alcohol from complete hydrogenation of cinnamaldehyde. The selectivity order of C=C bond hydrogenation followed Pt_1Co_2@Co cubes > Pt nanocubes > Pt/C > Pt_2Co_1 multicubes. Pt_2Co_1 cubes gave 51.3 % selectivity for unsaturated alcohol from C=O hydrogenation, which was higher than that of another three catalysts. The ability of catalytic hydrogenation for C=O bond was displayed in descending sequence: Pt_2Co_1 multicubes > Pt/C > Pt cubes > Pt_1Co_2@Co cubes.

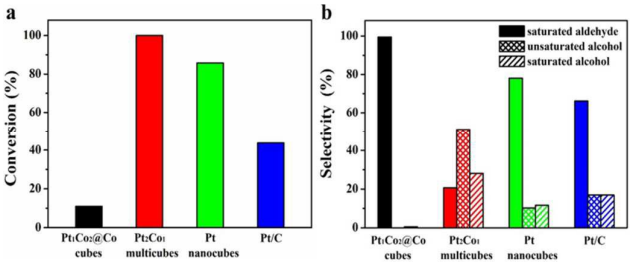

Fig. 5 (a) The catalytic activity of Pt_1Co_2@Co cubes, Pt_2Co_1 multicubes, Pt nanocubes and Pt/C for cinnamaldehyde hydrogenation. (b) Selectivity of

cinnamaldehyde hydorgenation over the four catalysts. (Reaction conditions: 60°C for 12 h in 2 MPa H_2)

The catalytic properties of Pt_1Co_2@Co cubes and Pt_2Co_1 multicubes should be attributed to their surface structure and compostion rather than electronic structure, since electronic properties of the above two catalysts showed no dramatic distinction. X-ray photoelectron spectroscopy (XPS) studies in Fig. 6 suggest that the structural difference of the core-shell and multicube structure did not bring about the charge transfer between Pt and Co. The shifts in Pt 4f bonding energy of both Pt_1Co_2@Co cubes and Pt_2Co_1 multicubes were not observed, compared to that of pure Pt (Fig. 6a). The Co 2p spectra of the two Pt-Co catalysts are located at the similar positions, as seen in Fig. 6b. The results give the fact that there is no remarkable discrepancy in the electronic structure between Pt_1Co_2@Co cubes and Pt_2Co_1 multicubes. Taken into consideration that the hydrogenation ability of Co is weeker than that of Pt, Pt_1Co_2@Co cubes show low catalytic activity and complete hydrogenation of C=C bond, in that they are not able to efficiently hydrogenate C=O bond of cinnamaldehyde. While Pt_2Co_1 multicubes have more concentration of Pt and are enclosed by some high-index facets such as {130}, which gives rise to the excellent catalytic activity. Meanwhile some cinnamaldehyde molecules have an opportunity into the spaces between the adjacent cubes of multicubes and then are hydrogenated on these areas. The steric effect created by the cinnamaldehyde molecules on the these uneven surfaces can not be neglected under this reaction condition, which might make the terminal C=O bond of cinnamaldehyde tends to be adsorbed on these uneven faces, leading to the hydrogenation of C=O bond more than that of C=C bond.

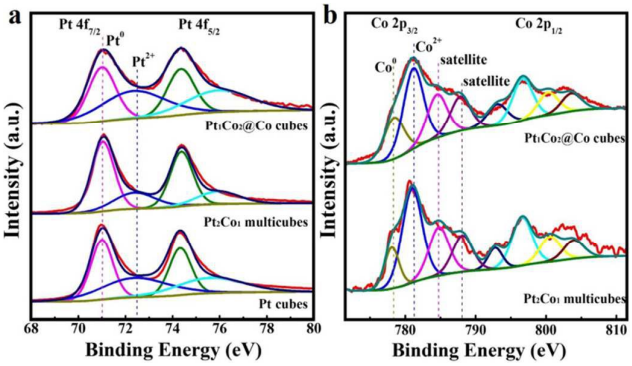

Fig. 6 (a) Pt 4f electron region of XPS profiles of Pt_1Co_2@Co cubes, Pt_2Co_1 multicubes and Pt cubes. (b) Co 2p electron region of XPS profiles of Pt_1Co_2@Co cubes and Pt_2Co_1 multicubes.

Conclusions

In summary, we have fabricated Pt_xCo_y@Co cubes and Pt_xCo_y multicubes through the previous structure as a seed precursor to induce the formation of the latter. Pt_xCo_y@Co cubes can be obtained by a site-selected deposition of Co atoms on the interstices between adjacent pods of the multipods, followed by a coating of Co atoms on the surface. Pt_xCo_y multicubes were made by the substitution Pt atoms for Co atoms as well as the interdiffusion between Pt atoms and Co atoms. Pt_xCo_y@Co cubes gave rise to complete selectivity towards C=C bond of unsaturated aldehyde and Pt_xCo_y multicubes exhibited the superior catalytic activity with higher selectivity for C=O group of unsaturated aldehyde, compared to pure Pt nanocubes and a commercial Pt/C catalyst. The ability to control the shape evolution induced by seed precursors will help us to optimise the design of nanocatalysts to tune their activities and selectivities for some chemical reactions.

Acknowledgements

We are grateful for financial support by National Natural Science Foundation of China (21273151) and Hundred Talent Program of CAS. Y.Z. acknowledges support by Ministry of Education for returning overseas Chinese scholars.

Notes and references

1 X. Liu, D. Wang and Y. Li, *Nano Today*, 2012, **7**, 448-466.
2 J. Wu, L. Qi, H. You, A. Gross, J. Li, and H. Yang, *J. Am. Chem. Soc.*, 2012, **134**, 11880-11883.
3 D. Zhang, J. Li, J. Kang, T. Chen, Y. Zhang, L. Wang and L Guo, *CrystEngComm*, 2014, **16**, 5331-5337.
4 Y. Wu, S. Cai, D. Wang, W. He and Y. Li, *J. Am. Chem. Soc.*, 2012, **134**, 8975−8981.
5 J. Wu and H. Yang, *Acc. Chem. Res.*, 2013, **46**, 1848-1857.
6 C. Chen, Y. Kang, Z. Huo, Z. Zhu, W. Huang, H. L. Xin, J. D. Snyder, D. Li, J. A. Herron, M. Mavrikakis, M. Chi, K. L. More, Y. Li, N. M. Markovic, G. A. Somorjai, P. Yang and V. R. Stamenkovic, *Science*, 2014, **343**, 1339-1343.
7 Y. Wu, D. Wang, G. Zhou, R. Yu, C. Chen and Y. Li, *J. Am. Chem. Soc.*, 2014, **136**, 11594-11597.
8 A. Oh, H. Baik, D. S. Choi, J. Y. Cheon, B. Kim, H. Kim, S. J. Kwon, S. H. Joo, Y. Jung and K. Lee, *ACS Nano*, 2015, **9**, 2856-2867.
9 X. Zhao, S. Chen, Z. Fang, J. Ding, W. Sang, Y. Wang, J. Zhao, Z. Peng and J. Zeng, *J. Am. Chem. Soc.*, 2015, **137**, 2804-2807.
10 Y. Wu, D. Wang, Z. Niu, P. Chen, G. Zhou and Y. Li, *Angew. Chem. Int. Ed.*, 2012, **51**, 12524-12528.
11 X. Xu, X. Zhang, H. Sun, Y. Yang, X. Dai, J. Gao, X. Li, P. Zhang, H. Wang, N. Yu and S. Sun, *Angew. Chem. Int. Ed.*, 2014, **53**, 12522-12527.
12 C. Cui, L. Gan, M. Neumann, M. Heggen, B. R. Cuenya and P. Strasser, *J. Am. Chem. Soc.*, 2014, **136**, 4813-4816.
13 R. Zheng, M. D. Porosoff, J. L. Weiner, S. Lu, Y. Zhu and J. G. Chen, *Appl. Catal. A-Gen.*, 2012, **419-420**, 126-132.
14 B. Wu, H. Huang, J. Yang, N. Zheng and G. Fu, *Angew. Chem.*, 2012, **124**, 3496-3499.
15 M. S. Ide, B. Hao, M. Neurock and R. J. Davis, *ACS Catal.*, 2012, **2**, 671-683.
16 W. Yan, Z. Guo, X. Jia, V. Kariwala, T. Chen and Y. Yang, *Chem. Eng. Sci.*, 2012, **76**, 26-36.
17 P. Gallezot and D. Richard, *Catal. Rev.*, 1998, **40**, 81-126.
18 Z. Rong, Z. Sun and Y. Wang, *Catal. Lett.*, 2014, **144**, 980-986.
19 S. Choi, S. Lee, W. Y. Kim, R. Choi, K. Hong, K. M. Nam, S. W. Han and J. T. Park, *ACS Appl. Mater. Inter.*, 2012, **4**, 6228-6234.
20 Y. Xia, Y. Xiong, B. Lim and S. E. Skrabalak, *Angew. Chem. Int. Ed.*, 2009, **48**, 60-103.
21 L. Zhang, W. Niu and G. Xu, *Nano Today*, 2012, **7**, 586-605.
22 B. Cordero, V. Gomez, A. E. Platero-Prats, M. Reves, J. Echeverria, E. Cremades, F. Barragan and S. Alvarez, *Dalton Trans.*, 2008, **37**, 2832-2838.

23 H. Zhang, M. Jin and Y. Xia, *Angew. Chem. Int. Ed.*, 2012, **51**, 7656-7673.